Bioconjugate Chemistry

Article

pubs.acs.org/bc

Biofunctionalized Gadolinium-Containing Prussian Blue Nanoparticles as Multimodal Molecular Imaging Agents

Matthieu F. Dumont,[†] Hilary A. Hoffman,[†] Pryscilla R. S. Yoon,[†] Laurie S. Conklin,[†,§] Shanta R. Saha,[‡] JohnPierre Paglione,[‡] Raymond W. Sze,[†,⊥] and Rohan Fernandes*[,†,§,⊥]

[†]The Sheikh Zayed Institute for Pediatric Surgical Innovation, Children's National Medical Center, 111 Michigan Avenue NW, Washington, DC 20010, United States

[‡]Center for Nanophysics and Advanced Materials, Department of Physics, University of Maryland, College Park, Maryland 20742, United States

[§]Department of Pediatrics and [⊥]Department of Radiology, George Washington University, 2330 Eye St NW, Washington, DC 20037, United States

Supporting Information

ABSTRACT: Molecular imaging agents enable the visualization of phenomena with cellular and subcellular level resolutions and therefore have enormous potential in improving disease diagnosis and therapy assessment. In this article, we describe the synthesis, characterization, and demonstration of core−shell, biofunctionalized, gadolinium-containing Prussian blue nanoparticles as multimodal molecular imaging agents. Our multimodal nanoparticles combine the advantages of MRI and fluorescence. The core of our nanoparticles consists of a Prussian blue lattice with gadolinium ions located within the lattice interstices that confer high relaxivity to the nanoparticles providing MRI contrast. The relaxivities of our nanoparticles are nearly nine times those observed for the clinically used Magnevist. The nanoparticle MRI core is biofunctionalized with a layer of fluorescently labeled avidin that enables fluorescence imaging. Biotinylated antibodies are attached to the surface avidin and confer molecular specificity to the nanoparticles by targeting cell-specific biomarkers. We demonstrate our nanoparticles as multimodal molecular imaging agents in an *in vitro* model consisting of a mixture of eosinophilic cells and squamous epithelial cells. Our nanoparticles specifically detect eosinophilic cells and not squamous epithelial cells, via both fluorescence imaging and MRI *in vitro*. These results suggest the potential of our biofunctionalized Prussian blue nanoparticles as multimodal molecular imaging agents *in vivo*.

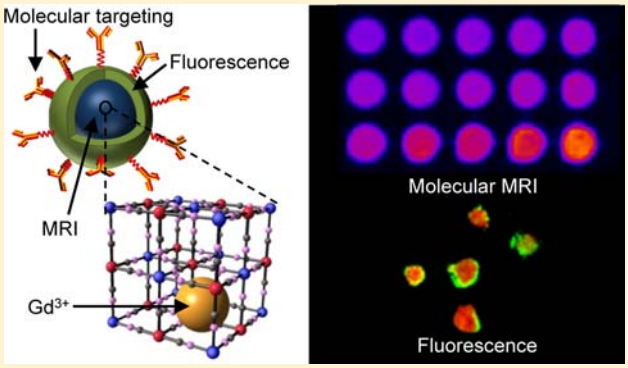

INTRODUCTION

Molecular imaging is the molecularly targeted, real-time, and noninvasive imaging of phenomena and processes at cellular and subcellular levels.[1] For enhanced visualization, molecular imaging typically involves the administration of an exogenous imaging agent, which can be in the form of a small molecule, engineered protein/antibody, or nanoparticle (NP).[2] The key attributes of an imaging agent include the ability to be molecularly targeted and the ability to be visualized using imaging techniques. Various clinical and preclinical imaging techniques explored in molecular imaging include CT, PET, SPECT, MRI, magnetic resonance spectroscopy, ultrasound, photoacoustic imaging, and optical imaging including bioluminescence, fluorescence, Raman, and intravital microscopy.[3] Each technique has limitations with respect to its spatial resolution, sensitivity, depth of penetration, and safety profile. Multimodal molecular imaging agents, capable of being detected by two or more imaging techniques, aim to combine the features and advantages of individual imaging techniques and overcome their limitations.[2,3] In addition to improved imaging capabilities, multimodal molecular imaging agents have the potential to impact clinical care by reducing or simplifying patient preparation steps required in clinical molecular imaging.

In this article, we describe biofunctionalized Prussian blue nanoparticles as molecular imaging agents that can be visualized using fluorescence and MRI. Fluorescence imaging was recently used in a clinical demonstration of fluorescence image-guided surgery where the fluorescence was used to intraoperatively highlight the resection margins of tumors.[4−6] Despite its promise as an imaging modality, fluorescence imaging is not widely used in a clinical setting. The vast majority of clinically used MRI contrast agents are based on gadolinium chelates that

Received: September 12, 2013
Revised: November 23, 2013
Published: December 11, 2013

   dx.doi.org/10.1021/bc4004266 | *Bioconjugate Chem.* 2014, 25, 129−137

typically provide positive contrast (hyperintensity) such as Magnevist and ProHance.[7,8] Other preclinical demonstrations of positive contrast agents include gadolinium chelated in cyclic oligomers,[9] vesicles loaded with gadolinium NPs,[10] gadolinium phosphate NPs,[11,12] copolymer-based gadolinium NPs,[13] human serum albumin NPs loaded with gadolinium chelates and coated with transferrin,[14] and citrate-capped Prussian blue NPs and their gadolinium-based analogues as positive contrast agents.[15,16] The other class of contrast agents approved for clinical use is based on iron oxide NPs. These agents provide negative contrast (hypointensity) and are predominantly used for hepatic imaging due to their natural propensity to accumulate in the liver.[17,18] Currently there are no approved molecular imaging agents for MRI. Clinically used MRI contrast agents are generally limited to anatomical resolutions. Furthermore, there are no approved multimodal, molecular imaging agents. We aim to fill this need by investigating biofunctionalized Prussian blue nanoparticles.

The rationale for pursuing nanoparticles is because they can be synthesized with tunable, multifunctional properties suitable for molecular targeting and imaging. Additionally, the imaging techniques used to visualize biofunctionalized Prussian blue nanoparticles, fluorescence and MRI, have complementary features. Fluorescence imaging provides high sensitivity ($\sim 10^{-9}$–10^{-12} M) but lower spatial resolution, while MRI provides high spatial resolution (~ 100 μm), limitless depths of penetration, but lower sensitivity ($\sim 10^{-3}$–10^{-5} M).[19]

The biofunctionalized Prussian blue NPs described here have a core–shell structure (Figure 1A). The core consists of a Prussian blue lattice containing interstitial gadolinium cations (GdPB), which function as MRI contrast agents. Prussian blue is a face-centered cubic network of iron(III) and iron(II) ions bridged by linear cyanide ligands (Figure 1B). In order to maintain charge balance within the framework, Prussian blue creates cyanometallate vacancies and incorporates interstitial cations. Prussian blue is an FDA-approved material that is marketed as Radiogardase to trap and retain radioisotopes of cesium and thallium. We exploit this "cation-trapping" feature to load Prussian blue nanoparticles with the paramagnetic ion Gd^{3+} and obtain an MRI contrast agent. GdPB NPs can be used both as a T_1 (hyperintensity) and T_2 (hypointensity) contrast agent as described later.

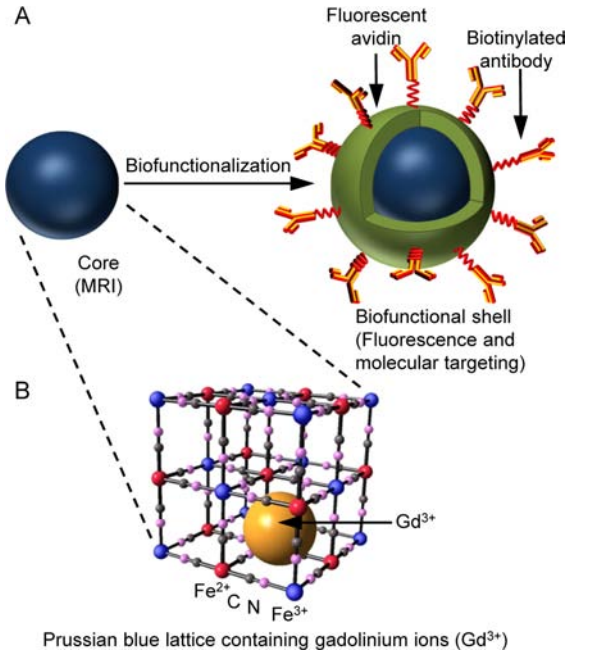

Figure 1. Biofunctionalized Prussian blue nanoparticles as multimodal molecular imaging agents. (A) Schematic representation of the core–shell nanoparticle consisting of an inorganic gadolinium-containing Prussian blue core (GdPB; providing MRI contrast), a biofunctional shell comprising fluorescent avidin (enabling fluorescent imaging) and biotinylated antibodies (for molecular targeting). (B) Ball-and-stick representation of the Prussian blue lattice containing interstitial Gd^{3+} ions (interstitial potassium ions are omitted for clarity).

The GdPB core is coated with a layer of the fluorescently labeled glycoprotein avidin that enables fluorescent imaging. Avidin also functions as an "interconnect" for attaching biotinylated molecular targeting ligands.[20] We employ the biofunctionalized Prussian blue NPs as multimodal molecular imaging agents in an *in vitro* model of the disease eosinophilic esophagitis (EoE). EoE is an inflammatory disease of the upper gastrointestinal tract marked by the abnormal infiltration of eosinophils into the esophagus.[21] The *in vitro* model of EoE consists of a mixture of an eosinophilic cell line (that represents the infiltrating eosinophils) and a squamous epithelial cell line (that represents the normal esophagus). The Prussian blue NPs are biofunctionalized with an antibody (anti-human eotaxin-3) that specifically targets eosinophils, not the squamous epithelium.[21] We describe in this article the synthesis, characterization, stability, cytotoxicity, fluorescence, and MR imaging capabilities of the biofunctionalized Prussian blue NPs. Further, we describe the results of using biofunctionalized Prussian blue NPs as multimodal molecular imaging agents.

EXPERIMENTAL PROCEDURES

Materials. Ultrapure water used in synthetic procedures was obtained from a Millipore Milli-Q system with a resistivity of at least 17.8 MΩ-cm. Reagents and chemicals were purchased from Sigma-Aldrich or Fisher-Acros and used without further purification.

GdPB Nanoparticle Synthesis. The synthesis was carried out at room temperature (RT). An aqueous solution of 4.9 mg $FeCl_2 \cdot 4H_2O$ (2.5×10^{-5} mol) in 5 mL of Milli-Q H_2O was added under vigorous stirring to an aqueous solution of 11.2 mg $Gd(NO_3)_3$ (2.5×10^{-5} mol) in 10 mL of Milli-Q H_2O followed by the addition of an aqueous solution containing 9.2 mg of $K_3Fe(CN)_6$ (2.8×10^{-5} mol) in 5 mL of Milli-Q H_2O. After stirring for 15 min, the precipitate is isolated by centrifugation (20 000 *g* for 5 min) and rinsed by sonication (5 s, high power) in Milli-Q H_2O. The isolation and rinsing steps are repeated three times before the particles are redispersed by sonication in Milli-Q Water. The synthesis yields a blue powder (85% yield). Chemical analysis by energy-dispersive X-ray spectroscopy (EDS) gives the following formula: $K_{0.53}Gd_{0.89}Fe^{III}_4[Fe^{II}(CN)_6]_{3.8} \cdot 1.2\ H_2O$. IR (KBr): 2074 cm^{-1} (m, ν_{CN}, Fe^{III}-NC-Fe^{II}).

GdPB Surface Modification with Avidin-Alexa Fluor 488 (GdPB-A488). Each molecule of fluorescent avidin holds 3 fluorophore molecules (Alexa Fluor 488; $\lambda_{excitation} = 497 \pm 5$ nm, $\lambda_{emission} = 521 \pm 5$ nm). A 900 μL dispersion of GdPB in Milli-Q water (0.18 mg/mL) and 100 μL Avidin-Alexa Fluor 488 solution (1 mg/mL, Life Technologies, Grand Island, NY, USA) were mixed by vortexing. The mixture was incubated, protected from light, on an orbital shaker at 4 °C for 3 h. The NPs were then washed three times with Milli-Q water and dispersed in 1 mL Milli-Q water.

dx.doi.org/10.1021/bc4004266 | *Bioconjugate Chem.* 2014, 25, 129–137

Surface Modification with Anti-Human Eotaxin-3 Antibody (GdPB-A488-Eot3). Goat anti-human eotaxin-3 (affinity purified, PeproTech, Inc., Rocky Hill, NJ, USA) was biotin-labeled using a ChromaLink Biotin One Shot antibody labeling kit (Solulink, San Diego, CA, USA). Proper labeling (biotin/antibody ratio 3:1) was verified using a ND-1000 Spectrophotometer (Nanodrop, Wilmington, DE, USA). A 900 μL dispersion of GdPB-A488 in Milli-Q water (0.18 mg.mL^{-1}) and 100 μL of biotinylated goat anti-human eotaxin-3 were mixed by vortexing. The mixture was incubated, protected from light, on an orbital shaker at 4 °C for 12 h. The NPs were then washed three times with Milli-Q water and dispersed in 1 mL Milli-Q water.

Transmission Electron Microscopy (TEM). TEM was performed on a JEM-2100 FEG high-resolution transmission electron microscope at 200 kV. The TEM grids (carbon film on a holey carbon support film, 400 mesh, copper from Ted-Pella, Inc.) were prepared by dropping, onto the grid, 20 μL of a solution containing 5 mg of sample dispersed by sonication in 2 mL of 70% EtOH for 3 min. Energy-dispersive X-ray spectroscopy (EDS) was performed with Oxford Instruments INCA 250 coupled to the HRTEM microscope. A total of 3 scans were performed on different parts of the sample and then averaged to give relative atomic percentages for gadolinium, potassium, and iron (Supporting Information). Chemical formulas were based on the metal composition from EDS, and were confirmed for overall electroneutrality of the compound.

Fourier Transform Infrared Spectrometry (FTIR). FTIR spectra were recorded on a Thermo Nicolet NEXUS 670 FTIR Spectrometer fitted with a Smart Endurance 0033−897 ATR accessory. Typically, 16 scans were taken between 800 cm^{-1} and 3200 cm^{-1} with a precision of 0.4 cm^{-1}. Powder GdPB nanoparticles were pressed against a zinc selenide (ZnSe) ATR anvil.

Powder X-ray Diffractometry. X-ray diffraction patterns were measured on a D8 Advance powder diffractometer using Cu Kα radiation from a sealed tube with a Ni β-filter equipped with Soller slits and a LynxEye position sensitive detector. GdPB nanoparticles were carefully packed (without excessive pressure) in a zero-background sample holder and measured from 10° to 50° 2θ with 0.013° step sizes and a 0.6 s/step exposition. Peak fitting was performed on the Topas software (Bruker AXS) using a fundamental parameters approach.

SQUID Magnetometry. Powder samples of GdPB nanoparticles, typically 10 to 20 mg, were immobilized in a gelatin capsule that was held in a plastic drinking straw for loading in a commercial SQUID magnetometer. Isothermal magnetization was measured at 1.8 K while sweeping the field between −70 kG and 70 kG. Temperature dependent sweeps were obtained after first cooling samples from 300 K in zero field, applying 50 Oe, and then performing measurements upon warming.

Phantom Preparation. The GdPB relaxivities (r_1 and r_2) were compared to commercial gadolinium chelate formulations (Magnevist, gadolinium diethylenetriamine pentaacetic acid, Bayer HealthCare Pharmaceuticals Inc., Wayne, NJ, 07470). GdPB standards were prepared with Gd^{3+} concentrations ranging from 5.0 × 10^{-5} to 1.52 × 10^{-9} M in 0.5% agarose solutions (Acros Organics, Pittsburgh, PA). PB standards were prepared in Fe concentrations chosen to be the same as Fe concentrations found in the GdPB dilutions and thus providing a baseline. Concentrations used ranged from 4.0 × 10^{-4} to 2.4 × 10^{-8} M in 0.5% agarose solutions (Acros Organics, Pittsburgh, PA). Magnevist standards were made using the same procedure, in Gd^{3+} concentrations ranging from 2.5 to 1.52 × 10^{-4} M. This range of concentrations was specifically chosen to be clinically relevant as per the manufacturer's specifications (0.1 mmol/kg body weight).[7] The solutions were introduced in 1.5 mL centrifuge tubes with an equal volume of agarose solution, subsequently mixed and cooled.

MR Relaxation Time Measurements. All MR measurements were performed at a constant temperature of 20 °C to allow for easy comparison with other studies, in a horizontal 3 T clinical magnet (GE Healthcare). The phantom was placed next to a solid block of 2% agar (150 cm^3) and secured at the center of an 8-channel HD brain coil (GE Healthcare). The spectrometer was interfaced with the built-in GE healthcare software. For each of the tested contrast agents, T_1 and T_2 relaxation times were measured in the same coronal 0.5-mm-thick slice, positioned at midheight of the wells. A variable inversion time (TI) inversion recovery sequence was used for T_1 measurements (variable TI = 50; 117; 432; 942; 1961; 4000 ms; repetition time (TR) = 10 000 ms; echo time (TE) = 6.6 ms; echo train (ET) = 22; matrix size = 288 × 288, FOV = 23 × 11 cm^2). T_2 was measured with a multiple spin−echo sequence (repetition time (TR) = 5000 ms; echo time echo train (ET) = 22, and variable TE= 12; 20; 35; 65; 125; 165; 245 ms, matrix size = 192 × 192, FOV = 22 × 22 cm^2).

MR Data Analysis. All MR data were analyzed using *ImageJ* (National Institutes of Health Bethesda, MD). For each sample, the signal intensity on acquired images was averaged within regions of interest (ROIs) and plotted against TI for T_1 inversion recovery curves or TE for T_2 decay curves. Data were then fitted to the following monoexponential function:

$$T_1\text{: (TR)} = A(1 - e^{(-TR/T_1)}) + y_O \quad (1)$$

$$T_2\text{: (TE)} = A(1 - e^{(-TE/T_2)}) + y_O \quad (2)$$

T_1 and T_2 values were transformed into R_1 and R_2 relaxation rates ($1/T_1$ (s^{-1}), $1/T_2$ (s^{-1})). Finally, R_1 and R_2 values were plotted against the concentration of the corresponding contrast agent, and r_1 and r_2 (mM^{-1} s^{-1}) relaxivities were obtained as the slope of the resulting linear plots.

Dynamic Light Scattering and Zeta Potential. The sizes and zeta potentials of 10 μg/mL suspensions, respectively, of GdPB, GdPB-A488, and GdPB-A488-Eot3 were determined using a Zetasizer Nano ZS (Malvern Instruments, Worcestershire, U.K.). Values of zeta potential were determined using the Smoluchowski diffusion equation.

Confocal Imaging. Lab-Tek chambered microscope slides (Nunc, Rochester, NY, USA) were covered by 400 μL of a 0.002% solution of poly(L-lysine) hydrobromide (Sigma-Aldrich, St. Louis, MO, USA) and left to coat for 90 min. The solution was subsequently removed and the slides were left to dry for 24 h. The squamous epithelial cell line OE-21 (Sigma-Aldrich, St. Louis, MO, USA) was grown on a polylysine coated slide for 72 h, stained with 5 μM CellTrace red-orange (Life Technologies, Grand Island, NY, USA) in PBS at 37 °C for 30 min, fixed with a 4% formaldehyde solution at RT for 10 min, and then incubated with 2.5 × 10^{-8} mg/cell NPs (5 μL from 0.5 mg/mL GdPB-A488-Eot3 or GdPB-A488) in 1% bovine serum albumin (BSA) for 60 min. After each step described above, the cells were rinsed with PBS. Previous immunochemistry studies on clinical samples have shown that the expression of eotaxin-3 antigens persist on the surface of

dx.doi.org/10.1021/bc4004266 | *Bioconjugate Chem.* 2014, 25, 129−137

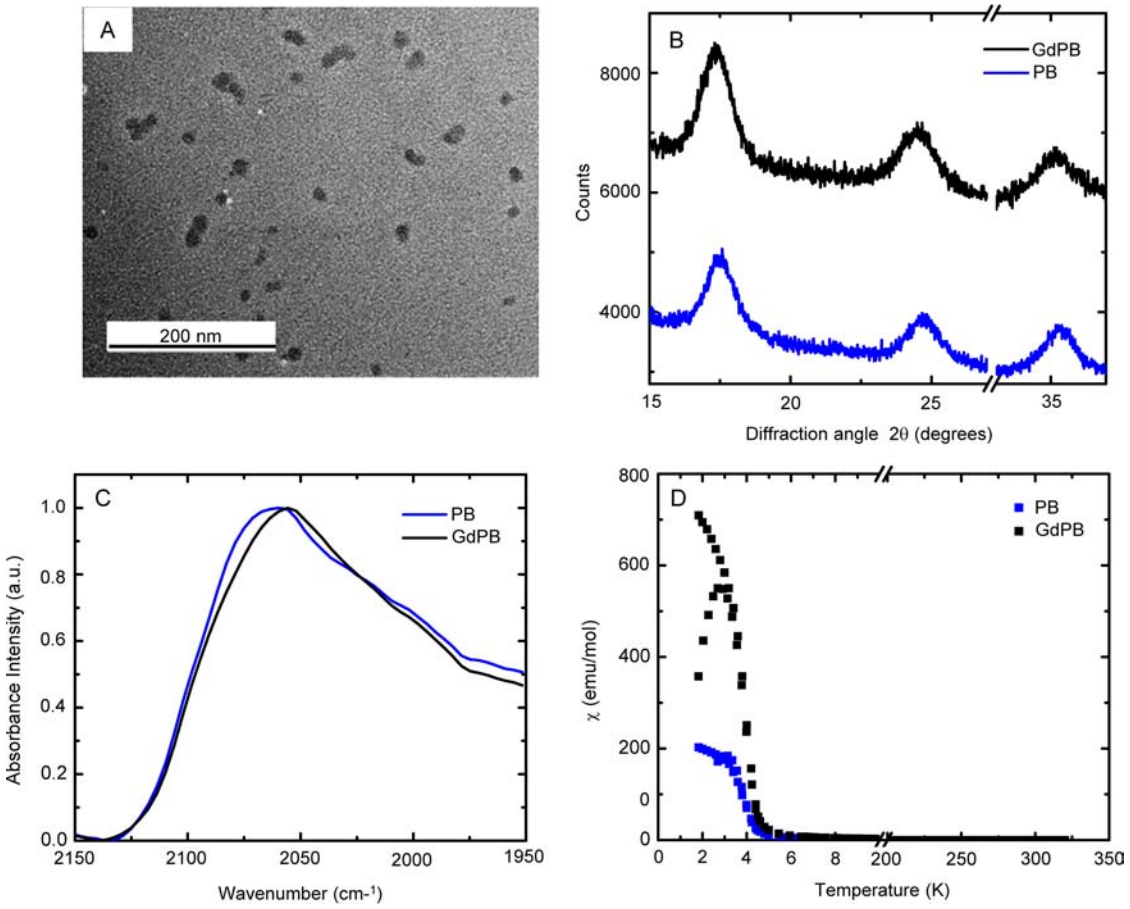

Figure 2. Physical and chemical characterization of the nanoparticle core. (A) Representative TEM image of the GdPB nanoparticles (Scale bar = 200 nm). (B) Room temperature XRD diffractogram of a sample of GdPB and Prussian blue without interstitial gadolinium (PB) particles with peaks around 17°, 24°, and 35°, corresponding to the 200, 220, and 400 diffraction planes, respectively. (C) FTIR spectra of GdPB (black line) and PB (blue line) in the cyanide stretching region (1900−2300 cm^{-1}). GdPB, similar to native Prussian blue (without gadolinium), features a broad band at 2070 cm^{-1} corresponding to the Fe^{II}-CN-Fe^{III} cyanide stretch energy.[22] (D) Magnetic susceptibility, χ, of GdPB (black symbols) and PB (blue symbols), measured at 50 G as a function of temperature.

the membrane even after fixing the cells.[21] The eosinophilic cell line EoL-1 (Sigma-Aldrich, St. Louis, MO, USA) was attached on a polylysine coated slide for 1 h at 37 °C in PBS, stained with 5 μM Calcein red-orange in PBS at 37 °C for 30 min, fixed with a 4% formaldehyde solution at RT for 10 min, and then incubated with 2.5×10^{-8} mg/cell NPs (5 μL from 0.5 mg/mL GdPB-A488-Eot3 or GdPB-A488) in 1% BSA for 60 min. After each step, the cells were rinsed with PBS. Images were acquired on a FV1000 confocal laser scanning microscope (Olympus, Center Valley, PA, USA).

Flow Cytometry. Mixtures of eosinophilic cells (EoL-1) and squamous epithelial cells (OE-21) in varying proportions were blocked with 5% BSA prior to adding the nanoparticles. After the blocking step, the cells were incubated with the NPs for 45 min. The cell mixtures were rinsed by successive centrifugation and redispersion cycles to remove any non-specifically bound NPs. Finally, the cells were fixed with 10% formaldehyde in neutral buffer before being stained with 7-Aminoactinomycin D. For fluorescence detection, cells were dispersed in PBS buffer. The specific binding of the NPs to the targeted cells was determined using flow cytometry by analyzing 10 000 cells from each sample on a FACSCalibur flow cytometer (BD Biosciences, San Jose, CA). The raw data was processed using the software FlowJo (Tree Star, Ashland, OR).

Molecular Magnetic Resonance Imaging. EoL-1 and OE-21 cells in a 1× PBS solution were added to 1.5 mL microcentrifuge tubes (for a total of 2.5 million cells per tube) that were arranged in rows (3) and columns (5). The first column had OE-21 cells only (2.5 million cells), the second column had a 3:1 ratio of OE-21 (1.875 million cells) to EoL-1 (0.625 million cells), the third column had a 1:1 ratio of OE-21 (1.25 million cells) to EoL-1 (1.25 million cells), the fourth column had a 1:3 ratio of OE-21 (0.625 million cells) to EoL-1 (1.875 million cells), and the fifth column had EoL-1 cells only (2.5 million cells). 50 μL of 1% BSA was added to each tube along with 100 μL of either GdPB-A488-Eot3 (0.18 mg/mL; row 1), GdPB-A488 (0.18 mg/mL; row 2), or saline solution (1× PBS; row 3). The tubes were vortexed, wrapped in foil, and then gently mixed on the orbital shaker at RT for 10 min. Next, 50 μL of 10% formaldehyde was added to each well; the tubes were vortexed, wrapped in foil, and placed on the orbital shaker to incubate for 10 min at RT. The tubes were then spun down in a microcentrifuge at 2100 rpm for 5 min. After removing the supernatant, each cell pellet was redispersed in 100 μL of Milli-Q water, which was then pipetted into individual wells on a 96 well plate with the same (column−row) orientation as described above for the tubes. 100 μL of 1% agarose was added to each well and their contents were thoroughly mixed.

dx.doi.org/10.1021/bc4004266 | Bioconjugate Chem. 2014, 25, 129−137

RESULTS

Synthesis and Biofunctionalization of the Gadolinium-Containing Prussian Blue Nanoparticles (GdPB). The first step in the biofunctionalized nanoparticle preparation is the synthesis of the core which consists of the gadolinium-containing Prussian blue NPs (GdPB). We achieve this in a one-pot, aqueous phase synthesis by adding ferrous chloride to a vigorously stirred mixture of potassium hexacyanoferrate (III) and gadolinium nitrate. Analysis of the resultant GdPB NPs using high-resolution TEM (HRTEM) shows individual nanoparticles with a mean nanoparticle size of 33 ± 7 nm (Figures 2A and Figure S1). The selected area electron diffraction (SAED) pattern taken at the edges of the agglomerate confirms that the lattice corresponds to Prussian blue (Figure S2).

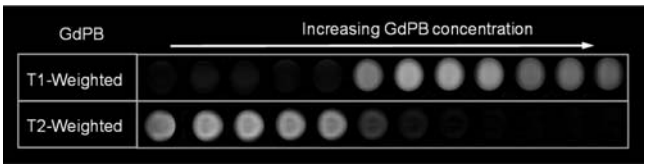

Figure 3. T1 and T2 weighted MR images at 3 T showing hyper and hypo intensity from GdPB. The concentration of gadolinium ([Gd^{3+}], in μM) is 0.72, 0.81, 0.9, 0.99, 1.0, 1.1, 1.2, 1.4, 1.5, 1.6, 1.7, and 1.8 μM from left to right. MR images were acquired using fast spin−echo sequences. (TE: 7 ms, ET: 22 ms, TR: 5000 for T1W and TE: 254 ms, ET:22 ms, TR: 5000 for T2W).

Powder X-ray diffraction from a sample of particles exhibits several groups of peaks corresponding to the 200, 220, and 400 diffraction planes at 17.36°, 24.46°, and 35.17°, respectively, for GdPB and 17.51°, 24.68°, and 35.29°, respectively, for Prussian blue without interstitial gadolinium (PB) (Figure 2B). These diffraction peaks can be indexed to Prussian blue lattices using the space group $Fm\bar{3}m$ (No. 225) and confirm the presence of one phase constituted by Prussian blue. Using the (400) reflections fitted to a Gaussian function, the lattice parameters for each compound are calculated. We find the following lattice constants: GdPB, a = 10.19 Å, and PB, a = 10.17 Å. No peaks corresponding to a mixed phase with different lattice parameters are detected, suggesting that both GdPB and PB are made up of the Prussian blue lattice.

The Fourier transform infrared (FTIR) spectrum of GdPB features a broad band at 2070 cm^{-1} corresponding to the Fe^{II}-CN-Fe^{III} cyanide stretch energy and matches the spectrum obtained for PB (Figure 2C).[22] It is important to note that the FTIR spectrum for GdPB does not display the noticeable double peak pattern at 2145 cm^{-1} and 2155 cm^{-1}, typical of gadolinium hexacyanoferrate ($KGd[Fe(CN)_6]\cdot nH_2O$) indicating that gadolinium is located in the interstitial sites of the Prussian blue lattice rather than covalently attached to the cyanide bonds that form the lattice (Figure S3).[23]

Samples of GdPB and PB particles show paramagnetic behavior and ordering below 5 K (Figure 2D). Using magnetic susceptibility, χ, measurements, a Curie−Weiss fit of the susceptibility for PB (S = 5/2 and g = 2) yields a Curie constant, C = 7.44 emu K/mol. A Curie−Weiss fit of the susceptibility for GdPB (S_1 = 7/2, S_2 = 5/2, and g = 2) yields a Curie constant, C = 16.49 emu K/mol (Figure S4A).[24] The magnetization, M_0, at 3 T is larger for GdPB than for PB and the value at saturation is 108.6 × 10^3 emuG mol^{-1} for GdPB and 50.1 × 10^3 emuG mol^{-1} for PB (Figure S4B). These results confirm that the presence of Gd^{3+} increases the volume magnetic susceptibility of GdPB compared to PB and predict that GdPB induces greater hypointensity than PB in T_2-weighted sequences.

The chemical composition of the material is confirmed by energy-dispersive X-ray spectroscopy (EDS) over areas covered by the NPs and by elemental analysis (Figure S5 and Table S1). The experimental formula derived $K_{0.53}Gd_{0.89}Fe^{III}_4[Fe^{II}(CN)_6]_{3.8}\cdot 1.2\ H_2O$, gives an average of 0.89 atoms of gadolinium per unit-cell. These data indicate that 1/8th of the Prussian blue interstitial sites are occupied with gadolinium cations.

The UV−vis spectrum of the GdPB shows a wide band around 700 nm, corresponding to the energy of the metal-to-metal charge transfer (MMCT) between Fe^{II} and Fe^{III} through the cyanide bridge (Figure S6). The maximum absorbance wavelength (λ_{max}) of the charge transfer band in GdPB is markedly red-shifted compared to a sample of Prussian blue (PB) where potassium ions (K^+) are not partly replaced by gadolinium ions (Gd^{3+}) (Supporting Information). The first derivative of the absorbance spectra give accurate values of the position of λ_{max}GdPB = 720 nm and λ_{max}PB = 695 nm. The redshift in GdPB is explained by changes in the electron density and orbital energies of the cyanide bonds due to the presence of gadolinium(III) in the lattice.[25,26]

We determine the longitudinal and transverse relaxivities (r_1 and r_2 values, respectively) of the NPs at a magnetic field strength of 3 T using serial dilutions (Figures S7 and S8). The longitudinal (r_1) and transverse (r_2) relaxivities are derived from linear fits of R_1 and R_2 versus gadolinium concentrations (Figure S9). The measurements are performed in triplicate with distinct batches of GdPB and PB particles. Relaxivity measurements with GdPB yield an r_1 value of 38.5 ± 4.6 $mM^{-1}\ s^{-1}$ and r_2 value of 44.7 ± 6.3 $mM^{-1}\ s^{-1}$. Simultaneous measurements are carried out with serial dilutions of the clinically used contrast agent Magnevist and Prussian blue without Gd^{3+} (PB). PB shows an r_1 value of 4.7 ± 3.6 $mM^{-1}\ s^{-1}$ and an r_2 value of 7.3 ± 6.6 $mM^{-1}\ s^{-1}$. Similarly, Magnevist shows an r_1 value of 4.3 ± 0.6 $mM^{-1}\ s^{-1}$ and an r_2 value of 5.0 ± 0.6 $mM^{-1}\ s^{-1}$. These values are in excellent agreement with

Table 1. Comparison of the Chemical Compositions and Magnetic Characteristics (Relaxivities, r_1 and r_2) of GdPB, Prussian Blue, and Magnevist

			relaxivity[b] ($mM^{-1}\ s^{-1}$)	
contrast agent	structure[a]	chemical composition	r_1	r_2
GdPB	NP	$K_{0.53}Gd_{0.89}Fe^{III}_4[Fe^{II}(CN)_6]_{3.8}\ 1.2\ H_2O$	38.5 ± 4.6	44.7. ± 6.3
PB (Prussian blue)	NP	$K_{0.8}Fe^{III}_4[Fe^{II}(CN)_6]_{3.2}\ 4.8\ H_2O$	4.7 ± 3.6	7.3 ± 6.6
Magnevist	C	$C_{28}H_{54}GdN_6O_{20}$	4.3 ± 0.6	5.0 ± 0.6

[a]NP: nanoparticles, C: chelate. [b]MR measurements were performed at 127 MHz (3 T).

dx.doi.org/10.1021/bc4004266 | Bioconjugate Chem. 2014, 25, 129−137

those reported in the literature.[27,28] The resultant r_1 and r_2 values obtained at 3 T for all samples are specified in Table 1 (and Table S2).

To determine the safety of the NPs as molecular imaging agents, we conduct chemical stability and cytotoxicity studies. Gd^{3+} release from the interstices of GdPB is investigated using xylenol orange titration as reported in related literature[11,29] and is determined to be negligible (Figure S10). A cell viability assay indicates no significant cytotoxicity of the NPs at concentrations lower than 0.5×10^{-6} mg/cell after 24 and 48 h for the eosinophilic cell line EoL-1. For the squamous epithelial cell line OE-21, no significant cytotoxicity was observed for all concentrations investigated at 24 h and no significant cytotoxicity at NP concentrations lower than 0.5×10^{-6} mg/cell after 48 h (Figure S11).

Using dynamic light scattering, we observe an increase in the hydrodynamic diameter (from 122 ± 36 nm, to 141 ± 42 nm, to 190 ± 57 nm; Figure 4B) and a change in the zeta potential

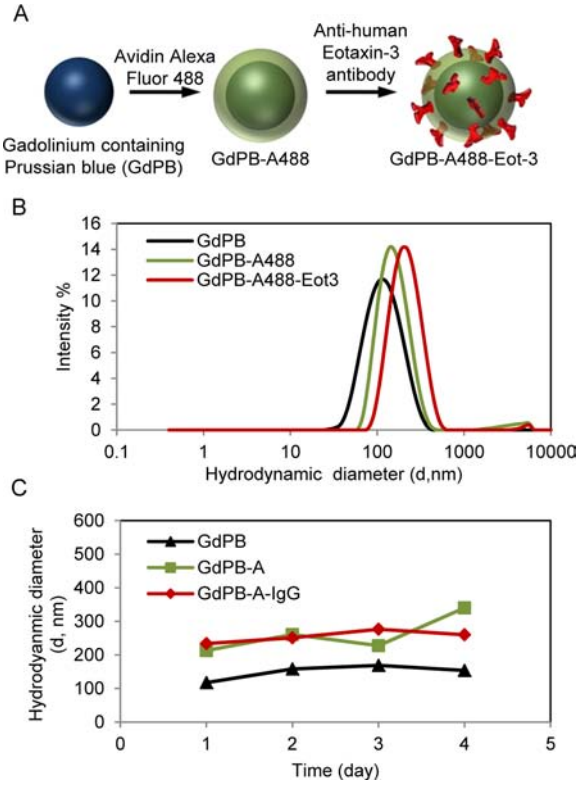

Figure 4. Biofunctionalization and stability of the nanoparticles. (A) Scheme depicting each step of the GdPB NP biofunctionalization (from GdPB to GdPB-A488-Eot3). (B) Size distributions of GdPB (blue), GdPB-A488 (green), and GdPB-A488-Eot3 (red) measured by dynamic light scattering (DLS). (C) Stability of GdPB (blue), GdPB-A (green), and GdPB-A-IgG (red) for up to 4 days postsynthesis quantified by DLS.

(from −35 mV, to −18 mV, to −21 mV) of the NP after each step of the synthesis and biofunctionalization—the GdPB core, addition of A488 to form GdPB-A488 and incubation with the anti-human eotaxin-3 antibody (GdPB-A488-Eot3). The particles are stable in both water (Figure 4C) and in medium (Figure S12) for up to 4 days post synthesis. The avidin binding capacity of GdPB is 400 μg avidin/mg GdPB (Figure S13), which indicates complete coverage of the nanoparticle surface. Furthermore, we estimate that approximately 92% of the avidin binding sites are available for binding by biotinylated ligands (Supporting Information). We measure the success and stability of the biofunctionalization of GdPB via temporal fluorescence studies (Figure S14).

Molecular Imaging Using the Biofunctionalized GdPB Nanoparticles. The *in vitro* model for testing the biofunctionalized GdPB NPs comprises an eosinophilic cell line EoL-1 and a squamous epithelial cell line OE-21. To investigate the NPs as fluorescence imaging agents, we add fixed amounts (2.5×10^{-8} mg/cell) of GdPB-A488-Eot3 (containing anti-human eotaxin-3 antibody) and GdPB-A488 controls (without antibody) to pure cultures of EoL-1 and OE-21. The GdPB-A488-Eot3 NPs specifically target the eosinophilic cell line (EoL-1) and not the squamous epithelial cells lines (OE-21) when visualized using confocal microscopy (Figure 5). Control GdPB-A488 NPs (without antibody) show little to no binding to both EoL-1 and OE-21 as evidenced by the lack of green fluorescence in these images (Figures 5A–C).

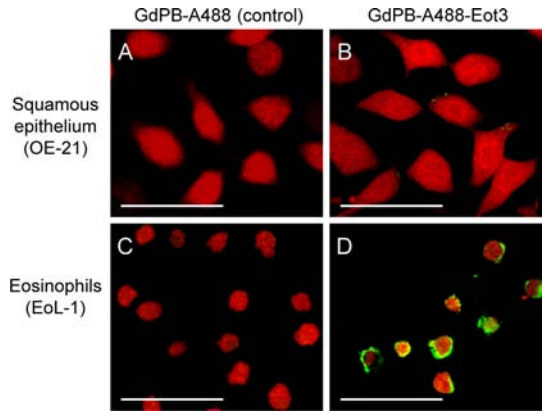

Figure 5. Nanoparticles specifically target eosinophils. Laser scanning confocal microscopy images of (A) squamous epithelial cells (OE-21) treated with control GdPB-A488, (B) OE-21 treated with GdPB-A488-Eot3, (C) eosinophilic cells (EoL-1) treated with control GdPB-A488, and (D) EoL-1 treated with GdPB-A488-Eot3. Microscope settings and acquisition parameters are identical for all images to allow for direct comparison of the fluorescence intensities. The intense green fluorescence in (D) suggests that GdPB-A488-Eot3 is able to specifically target the eotaxin-3 receptors on the eosinophils (scale bar = 50 μm).

To test the sensitivity of eosinophil detection using fluorescence, we add GdPB-A488-Eot3 to pure cultures of EoL-21 and OE-21 and mixtures of the two cell lines (OE-21:EoL-1 in varying proportions 3:1, 1:1, and 1:3). Using flow cytometry, we measure the percentage of the population that is fluorescently labeled by The NPs (% A488 positive; Figure 6). The GdPB-A488-Eot3 NPs specifically bind to eosinophils (EoL-1; 100% fluorescent; Figure 6E) but not to squamous epithelial cells (OE-21; 0% fluorescent; Figure 6A). When added to mixtures of eosinophils and squamous epithelial cells, the percentage of fluorescent cells increases with increasing amounts of eosinophils in the mixture—3:1, 1:1, and 1:3 of OE-21:EoL-1 ratios yield 47.0%, 68.2%, and 88.7% fluorescent cells, respectively (Figures S15 and S16).

To investigate GdPB-A488-Eot3 NP's as molecular MRI agents, we add fixed amounts (0.18 mg) of GdPB-A488-Eot3 NPs and controls (GdPB-A488 and saline) to either pure OE-21 (squamous epithelial cells), pure EoL-1 (eosinophils), or mixtures of OE-21 and EoL-1 (in 3:1, 1:1, and 1:3 OE-21:EoL-

dx.doi.org/10.1021/bc4004266 | Bioconjugate Chem. 2014, 25, 129–137

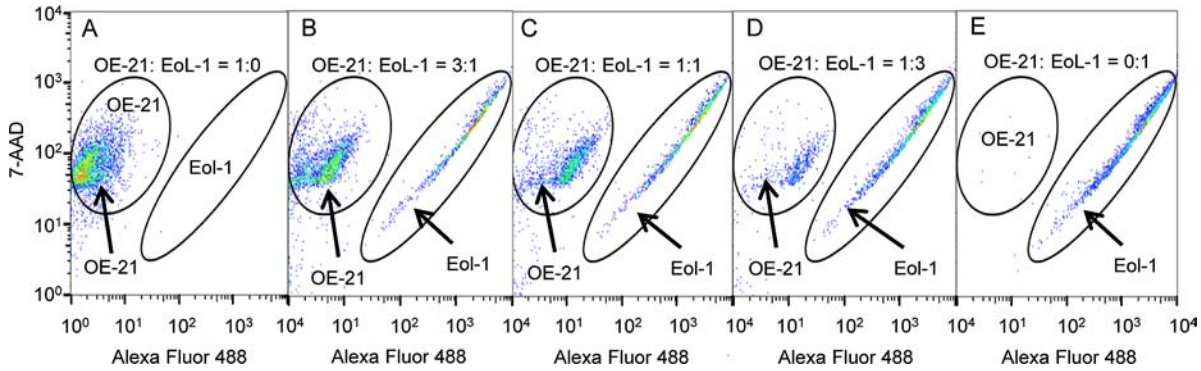

Figure 6. Flow cytometric analysis of nanoparticle specificity. Scatter plot of 7-AAD (cell stain) versus Alexa Fluor 488 (fluorophore on GdPB NPs). The gating identifies the eosinophilic cell line (EoL-1) and the squamous epithelial cell line (OE-21) and mixtures containing varying proportions of OE-21 and EoL-1 treated with identical amounts of GdPB-A488-Eot3.

1 ratios). The total number of cells per well is fixed (2.5 million cells/well). The GdPB-A488-Eot3 NPs bound marginally to OE-21 (72 units of contrast on a color scale normalized from 0 to 255; Figure 7) but bound to EoL-1 with higher specificity

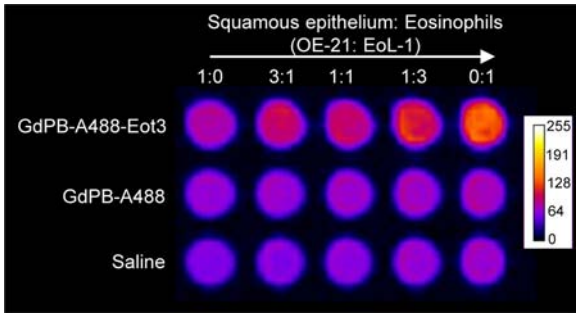

Figure 7. Nanoparticles allow quantitative detection of eosinophils by MRI at 3 T. (A) MRI phantom of GdPB-A488-Eot3, GdPB-A488, and saline added to suspensions containing varying ratios of squamous epithelial cells (OE-21) and eosinophils (EoL-1) (OE-21:EoL-1 ratios used were 1:0, 3:1, 1:1, 3:1, and 0:1). The amounts of the nanoparticles added are constant for all samples.

(127 units of contrast, an increase of 55 units at 3 T under the scanning parameters used). In mixtures of OE-21 and EoL-1 treated with GdPB-A488-Eot3, the MRI contrast increases with increasing amounts of EoL-1 cells in the mixture (contrast values for 3:1, 1:1, and 1:3; OE-21:EoL-1 ratios were 82, 88, and 103, respectively). Controls (GdPB-A488 and saline) show background levels of contrast, i.e., ∼60 contrast units.

DISCUSSION

Synthesis and Physical Properties of GdPB. Prussian blue is most commonly synthesized by reacting aqueous solutions of ferrous chloride ($Fe^{II}Cl_2$) and potassium hexacyanoferrate ($K_3Fe^{III}(CN)_6$), which readily precipitate to form colloidal solutions of Prussian blue nanoparticles. To ensure charge neutrality of the compound, Prussian blue incorporates cations available in its environment within its lattice. Incorporation of cations within the lattice can occur during or after the formation of the lattice. This property of the incorporation of cations within the Prussian blue lattice postlattice formation is the basis of its commercialization as Radiogardase. In the event of radiological contamination, Prussian blue administered as Radiogardase is ingested and traps radioactive isotopes, typically cesium or thallium, within its lattice and is rapidly eliminated by the body reducing exposure to radiation. Here, we produce GdPB nanoparticles that safely contain an MRI contrast agent by incorporating Gd^{3+} ions within the Prussian blue lattice during synthesis (via $Gd^{III}(NO_3)_3$ addition; Figure 1).

Crystallographic data (XRD and SAED) confirms GdPB having nearly identical structure and lattice parameters to Prussian blue (PB; Figure 2). Spectrometric measurement of the MMCT energy in UV−vis, and stretching energy of the cyanide bond in FTIR, confirms that we retain the repeating unit Fe^{II}-CN-Fe^{III} in both PB and GdPB. The presence of gadolinium retained in the lattice after purification of the particles is measured by EDS and further established by a dramatic increase in the magnetic susceptibility and relaxivities values (Figures 2 and 3). This comprehensive characterization of GdPB shows the presence of gadolinium and an intact PB structure, suggesting that the Gd^{3+} cations are not altering the Prussian blue lattice structure and are most likely contained within the interstitial vacancies (tetragonal sites of the lattice).

While commercial contrast agents containing Gd^{3+} are typically used solely as positive contrast agents,[7,8] the GdPB NPs presented in this study possess both positive and negative MRI contrast enhancing capabilities (Figure 3). This observation is confirmed by the generation of positive contrast on a clinical GE T_1-weighted image sequence (FLAIR, ET: 7; TR: 2300; TE: 24.4) and negative contrast on a clinical GE T_2-weighted image sequence (FRFSE, ET: 21; TR: 3500; TE: 104.1) at 3 T (Figure 3). Additionally, we calculate that the GdPB NPs demonstrate a 9-fold increase in MRI signal intensity when compared with the clinically used contrast agent Magnevist in both T_1- and T_2-weighted sequences (Figure 3 and Table 1). This establishes the efficiency of GdPB as an MRI contrast agent.

The generation of both T_1 and T_2 may be explained by contributions from two relaxation mechanisms. First, the contribution of protons, from coordinated or interstitial water molecules located in the particles, interacting with gadolinium cations through an inner-sphere mechanism gives positive contrast (hyperintensity) in T_1-weighted images. Second, the presence of Gd^{3+} in the Prussian blue lattice increases the overall spin density and the magnitude of the paramagnetism of the particles compared to Prussian blue, as confirmed by magnetometry studies. The presence of a paramagnetic particle disturbing the local magnetic field in its vicinity generates negative contrast (hypointensity) in T_2-weighted images. Incorporating Gd^{3+} in the Prussian blue lattice increases its

dx.doi.org/10.1021/bc4004266 | Bioconjugate Chem. 2014, 25, 129−137

strength as a T_2 contrast agent. The capability to generate hyper- and hypointensity with the same contrast agent is highly desirable when trying to increase the relative contrast sensitivity by image subtraction or to obtain T_1- and T_2-weighted images with a unique contrast agent.

Biofunctionalization of GdPB and Molecular Imaging. The biofunctional shell consists of the positively charged avidin that is fluorescently labeled with Alexa Fluor 488 and biotinylated anti-human eotaxin-3 antibody (Figure 4). The surface of the GdPB is negatively charged (the measured surface zeta potential is −35 mV), which electrostatically stabilizes the particles in suspension without need for surfactants.[30,31] The hexacyanoferrate-rich surface of the GdPB particles permits stable attachment of the highly positively charged glycoprotein avidin by electrostatic self-assembly.[32,33] GdPB NPs are coated with a layer of Alexa Fluor 488 labeled avidin (A488). The surface of GdPB-A488 is then modified with the biotinylated anti-human eotaxin-3 antibody using avidin−biotin interactions (Figure 4A). The interaction between avidin and biotin is one of the strongest noncovalent interactions known (K_d = 10^{-15} M)[34−36] and can withstand extremes of temperature, pH, and denaturing agents.[37−39] Anti-human eotaxin-3 antibody specifically binds to antigens on the eosinophilic cell line (EoL-1) conferring molecular targeting capabilities to GdPB. By using avidin−biotin interactions, we ensure robust attachment of the targeting antibody and maximize the efficiency and selectivity of the biofunctionalized nanoparticles for molecular imaging.

The utility of the biofunctionalized GdPB NPs for fluorescence imaging is evaluated by confocal microscopy (Figure 5) and flow cytometry (Figure 6). The particles are introduced to mixtures of an eosinophilic cell line (EoL-1) and a squamous epithelial cell line (OE-21). Control NPs (GdPB-A488), without antibody for molecular targeting, show little to no binding to both EoL-1 and OE-21 as evidenced by the lack of fluorescence signals observed in the confocal images (Figure 5) and flow cytometry (Figure 6). These results indicate the suitability of the biofunctionalized PB NPs for fluorescent detection of a population of eosinophils in a mixture of cells *in vitro*. The sensitivity limits of the biofunctionalized GdPB NPs for molecular MRI is tested at 3 T, in a clinical magnet by gradually reducing the proportion of target cells (Eol-1) in a mixture containing control OE-21 cells (Figure 7). These data show that we can detect the presence of target eosinophils in concentrations as low as 0.625 million EoL-1 cells out of a total of 2.5 million cells using GdPB-A488-Eot3 as molecular MRI agents.

CONCLUSION

We have described the synthesis of biofunctionalized NPs as multimodal molecular imaging agents (fluorescence and MRI). The biofunctionalized NPs have a core−shell structure comprising an "MR-imageable" Prussian blue core containing gadolinium within its interstices and a biofunctional shell consisting of fluorescent avidin and biotinylated anti-human eotaxin-3, enabling molecular targeting of eosinophils *in vitro*.

As an MRI contrast agent, biofunctionalized GdPB NPs demonstrate a 9-fold increase in MRI signal intensity when compared with the contrast agent Magnevist at clinically relevant concentrations in both T_1- and T_2-weighted sequences. Studies conducted *in vitro* using a mixture of cells lines demonstrate the feasibility of using GdPB NPs for fluorescence and MRI detection of a specific cell population and, consequently, the potential of the biofunctionalized GdPB NPs for multimodal molecular imaging *in vivo*. Studies developing these biofunctionalized NPs as a multimodal, molecular imaging agent in a mouse model are currently underway.

ASSOCIATED CONTENT

Supporting Information

Transmission electron microscopy (TEM); Fourier transform infrared spectroscopy (FTIR); SQUID magnetometry; chemical analysis; UV−vis spectroscopy; MRI characterization of GdPB; measurement of r_1 and r_2 relaxivities; chemical stability, cytotoxicity, and colloidal stability of GdPB; avidin and biotinylated ligand binding capacity of GdPB; stability of GdPB biofunctionalization; flow cytometry; and SI references. This material is available free of charge via the Internet at http://pubs.acs.org.

AUTHOR INFORMATION

Corresponding Author

*E-mail: RFernand@childrensnational.org. Phone (202) 476-5290.

Notes

The authors declare no competing financial interest.

ACKNOWLEDGMENTS

This work was supported by the Sheikh Zayed Institute for Pediatric Surgical Innovation's RAC Awards (# 30001489 and # 30000174). The authors gratefully acknowledge J. Nazarian, L. Chakrabarti, and S. Yadavilli from Children's National Medical Center for assistance with confocal microscopy, flow cytometry, and immunology studies. The authors acknowledge the support of The Maryland NanoCenter at University of Maryland and its NispLab. The NispLab is supported in part by the NSF as a MRSEC Shared Experimental Facility. The authors acknowledge S. Taylor from the Department of Chemistry at University of Maryland Optical Instrumentation Facility for the FTIR spectroscopy studies as well as D. Taylor and P. Y. Zavalij at the X-ray Crystallographic Center, Department of Chemistry and Biochemistry, University of Maryland, College Park, MD, for experimental data and analysis.

REFERENCES

(1) Meade, T. J., and Aime, S. (2009) Chemistry of molecular imaging. *Acc. Chem. Res. 42*, 821−821.

(2) James, M. L., and Gambhir, S. S. (2012) A molecular imaging primer: modalities, imaging agents, and applications. *Physiol. Rev. 92*, 897−965.

(3) Louie, A. (2010) Multimodality imaging probes: design and challenges. *Chem. Rev. 110*, 3146−3195.

(4) van Dam, G. M., Themelis, G., Crane, L. M. A., Harlaar, N. J., Pleijhuis, R. G., Kelder, W., Sarantopoulos, A., de Jong, J. S., Arts, H. J. G., van der Zee, A. G. J., Bart, J., Low, P. S., and Ntziachristos, V. (2011) Intraoperative tumor-specific fluorescence imaging in ovarian cancer by folate receptor-α targeting: first in-human results. *Nat. Med. 17*, 1315−1319.

(5) Chekina, N., Horák, D., Jendelová, P., Trchová, M., Beneš, M. J., Hrubý, M., Herynek, V., Turnovcová, K., and Syková, E. (2011) Fluorescent magnetic nanoparticles for biomedical applications. *J. Mater. Chem. 21*, 7630−7639.

(6) Frangioni, J. V. (2008) New technologies for human cancer imaging. *J. Clin. Oncol. 26*, 4012−4021.

(7) Http://bayerimaging.com/products/magnevist/.

(8) Http://imaging.bracco.com/us-en/products-and-solutions/contrast-media/prohance.
(9) Liang, G., Ronald, J., Chen, Y., Ye, D., Pandit, P., Ma, M. L., Rutt, B., and Rao, J. (2011) Controlled self-assembling of gadolinium nanoparticles as smart molecular magnetic resonance imaging contrast agents. *Angew. Chem., Int. Ed. 50*, 6283−6286.
(10) Broz, P., Ben-Haim, N., Santini, F., Marsch, S., Scheffler, K., Meier, W., and Hunziker, P. (2009) Nano imaging technologies: polymer vesicles loaded with precipitated gadolinium nanoparticles: a novel target-specific contrast agent for magnetic resonance imaging. *Eur. J. Nanomedicine 2*, 3−49.
(11) Hifumi, H., Yamaoka, S., Tanimoto, A., Citterio, D., and Suzuki, K. (2006) Gadolinium-based hybrid nanoparticles as a positive MR contrast agent. *J. Am. Chem. Soc. 128*, 15090−15091.
(12) Dumont, M. F., Baligand, C., Li, Y., Knowles, E. S., Meisel, M. W., Walter, G. A., and Talham, D. R. (2012) DNA surface modified gadolinium phosphate nanoparticles as MRI contrast agents. *Bioconjugate Chem. 23*, 951−957.
(13) Hou, S., Tong, S., Zhou, J., and Bao, G. (2012) Block copolymer-based gadolinium nanoparticles as MRI contrast agents with high T1 relaxivity. *Nanomedicine 7*, 211−218.
(14) Korkusuz, H., Ulbrich, K., Welzel, K., Koeberle, V., Watcharin, W., Bahr, U., Chernikov, V., Knobloch, T., Petersen, S., Huebner, F., Ackermann, H., Gelperina, S., Kromen, W., Hammerstingl, R., Haupenthal, J., Gruenwald, F., Fiehler, J., Zeuzem, S., Kreuter, J., Vogl, T. J., and Piiper, A. (2013) Transferrin-coated gadolinium nanoparticles as MRI contrast agent. *Mol. Imaging Biol. 15*, 148−154.
(15) Shokouhimehr, M. (2010) *Prussian Blue Nanoparticles and Its Analogues as New-Generation T1-Weighted MRI Contrast Agents for Cellular Imaging*, Kent State University.
(16) Shokouhimehr, M., Soehnlen, E. S., Hao, J., Griswold, M., Flask, C., Fan, X., Basilion, J. P., Basu, S., and Huang, S. D. (2010) Dual purpose prussian blue nanoparticles for cellular imaging and drug delivery: a new generation of T1-weighted MRI contrast and small molecule delivery agents. *J. Mater. Chem. 20*, 5251−5259.
(17) Bulte, J. W. M., and Kraitchman, D. L. (2004) Iron oxide MR contrast agents for molecular and cellular imaging. *NMR Biomed. 17*, 484−499.
(18) Morana, G., Salviato, E., and Guarise, A. (2007) Contrast agents for hepatic MRI. *Cancer Imaging 7*, S24−27.
(19) Aime, S., Castelli, D. D., Crich, S. G., Gianolio, E., and Terreno, E. (2009) Pushing the sensitivity envelope of lanthanide-based magnetic resonance imaging (MRI) contrast agents for molecular imaging applications. *Acc. Chem. Res. 42*, 822−831.
(20) Sapsford, K. E., Algar, W. R., Berti, L., Gemmill, K. B., Casey, B. J., Oh, E., Stewart, M. H., and Medintz, I. L. (2013) Functionalizing nanoparticles with biological molecules: developing chemistries that facilitate nanotechnology. *Chem. Rev. 113*, 1904−2074.
(21) Dellon, E. S., Chen, X., Miller, C. R., Woosley, J. T., and Shaheen, N. J. (2012) Diagnostic utility of major basic protein, eotaxin-3, and leukotriene enzyme staining in eosinophilic esophagitis. *Am. J. Gastroenterol. 107*, 1503−1511.
(22) Nakamoto, K. (2009) *Infrared and Raman Spectra of Inorganic and Coordination Compounds*, 6th ed., Wiley, Hoboken, NJ.
(23) Zhou, X., Wong, W.-T., Faucher, M. D., and Tanner, P. A. (2008) Crystallographic and infrared spectroscopic study of bond distances in Ln[Fe(CN)(6)]·4H(2)O (Ln = Lanthanide). *J. Solid State Chem. 181*, 3057−3064.
(24) Uemura, T., Ohba, M., and Kitagawa, S. (2004) Size and surface effects of prussian blue nanoparticles protected by organic polymers. *Inorg. Chem. 43*, 7339−7345.
(25) Wojdeł, J. C., and Bromley, S. T. (2006) Band gap variation in prussian blue via cation-induced structural distortion. *J. Phys. Chem. B 110*, 24294−24298.
(26) Cafun, J.-D., Champion, G., Arrio, M.-A., dit Moulin, C. C., and Bleuzen, A. (2010) Photomagnetic CoFe Prussian blue analogues: role of the cyanide ions as active electron transfer bridges modulated by cyanide−alkali metal ion interactions. *J. Am. Chem. Soc. 132*, 11552−11559.
(27) Pintaske, J., Martirosian, P., Graf, H., Erb, G., Lodemann, K.-P., Claussen, C. D., and Schick, F. (2006) Relaxivity of gadopentetate dimeglumine (magnevist), gadobutrol (gadovist), and gadobenate dimeglumine (multihance) in human blood plasma at 0.2, 1.5, and 3 T. *Invest. Radiol. 41*, 213−221.
(28) Runge, V. M., Biswas, J., Wintersperger, B. J., Baumann, S. S., Jackson, C. B., Herborn, C. U., and Patel, T. (2006) The efficacy of gadobenate dimeglumine (Gd-BOPTA) at 3 T in brain magnetic resonance imaging. *Invest. Radiol. 41*, 244−248.
(29) Barge, A., Cravotto, G., Gianolio, E., and Fedeli, F. (2006) How to determine free Gd and free ligand in solution of Gd chelates. a technical note. *Contr. Media Mol. Imaging 1*, 184−188.
(30) Dumont, M. F., Knowles, E. S., Guiet, A., Pajerowski, D. M., Gomez, A., Kycia, S. W., Meisel, M. W., and Talham, D. R. (2011) Photoinduced magnetism in core/shell prussian blue analogue heterostructures of KjNik[Cr(CN)6]l·nH2O with RbaCob[Fe(CN)-6]c·mH2O. *Inorg. Chem. 50*, 4295−4300.
(31) Catala, L., Brinzei, D., Prado, Y., Gloter, A., Stéphan, O., Rogez, G., and Mallah, T. (2009) Core−multishell magnetic coordination nanoparticles: toward multifunctionality on the nanoscale. *Angew. Chem., Int. Ed. 48*, 183−187.
(32) Jaiswal, J. K., Mattoussi, H., Mauro, J. M., and Simon, S. M. (2002) Long-term multiple color imaging of live cells using quantum dot bioconjugates. *Nat. Biotechnol. 21*, 47−51.
(33) Goldman, E. R., Balighian, E. D., Mattoussi, H., Kuno, M. K., Mauro, J. M., Tran, P. T., and Anderson, G. P. (2002) Avidin: a natural bridge for quantum dot-antibody conjugates. *J. Am. Chem. Soc. 124*, 6378−6382.
(34) Orita, T., Tomita, M., Harada, M., and Kato, K. (2012) Binding activity of avidin to the biotin within mesoporous silica materials for bioanalytical applications. *Anal. Biochem. 425*, 1−9.
(35) Bayer, E. A., and Wilchek, M. (2006) The Use of the Avidin-Biotin Complex as a Tool in Molecular Biology. In *Methods of Biochemical Analysis* (Glick, D., Ed.) pp 1−45, Vol. *26*, John Wiley & Sons, Inc., Hoboken, NJ, USA.
(36) DeLange, R. J., and Huang, T. S. (1971) Egg White Avidin. 3. Sequence of the 78-residue middle cyanogen bromide peptide. complete amino acid sequence of the protein subunit. *J. Biol. Chem. 246*, 698−709.
(37) Sun, S., Huang, X., Ma, M., Qiu, N., Cai, Z., Luo, Z., and Alies, N. P. (2012) Systematic evaluation of avidin−biotin interaction by fluorescence spectrophotometry. *Spectrochim. Acta, Part A 89*, 99−104.
(38) Green, N. M. (1963) Avidin. 4. Stability at extremes of pH and dissociation into sub-units by guanidine hydrochloride. *Biochem. J. 89*, 609−620.
(39) Fraenkel-Conrat, H., Snell, N. S., and Ducay, E. D. (1952) Avidin. II. Composition and mode of action of Avidin A. *Arch. Biochem. Biophys. 39*, 97−107.